

2D-layered Ti₃C₂ MXenes for Promoted Synthesis of NH₃ on P25 Photocatalysts

**Yuan Liao^a, Jing Qian^a, Gang Xie^a, Qing Han^{b, c}, Wenqiang Dang^c, Yuanshen Wang^a,
Lingling Lv^d, Sen Zhao^a, Lei Luo^a, Wen Zhang^a, Hai-Ying Jiang^{a,*}, Junwang Tang^{b,*}**

^a Key Lab of Synthetic and Natural Functional Molecule Chemistry of Ministry of Education, and the Energy and Catalysis Hub, College of Chemistry and Materials Science, Northwest University, Xi'an 710127, People's Republic of China

^b Department of Chemical Engineering, University College London, Torrington Place, London WC1E 7JE, U.K.

^c Department of Physics, Tianshui Normal University, Tianshui, Gansu, 741001, People's Republic of China.

^d College of Chemical Engineering and Technology, Tianshui Normal University, Tianshui, Gansu, 741001, People's Republic of China.

^e School of Chemistry, Beijing Institute of Technology, Beijing 100081, People's Republic of China.

jianghy@nwu.edu.cn, junwang.tang@ucl.ac.uk

Abstract

A kind of 2D-layered material, Ti_3C_2 MXenes, was successfully used as a new and efficient co-catalyst to improve the photocatalytic NH_3 synthesis performance of P25, due to its large surface area/2D-layered structure, large electric capacity, excellent electrical conductivity and effective chemisorption/activation of N_2 molecules. The generation yield of NH_3 was improved by 5 times on the optimized sample of 6% Ti_3C_2 MXenes-P25 compared with pure P25 under full spectrum light irradiation, consistent with the measured both photocurrent densities and charge lifetime. The further mechanistic study showed that Ti_3C_2 MXenes played an important role in the separation of photogenerated electron-hole pairs by accumulating the excited electrons from the excited P25. Most importantly, Ti_3C_2 MXenes could dramatically improve chemisorption and activation of N_2 as demonstrated by ESR spectra and DFT calculations. In addition, Ti_3C_2 MXenes loading on P25 could introduce oxygen vacancies in P25, also beneficial for photocatalytic NH_3 synthesis. Thus this study provides an efficient and promising co-catalyst for the photocatalytic NH_3 synthesis process from N_2 in air

1. Introduction

Artificial synthesis of NH_3 through low-cost N_2 is a matter of cardinal significance for modern agricultural production [1]. Haber-Bosch process dominated the industrial production of NH_3 over the past century. However, this process requires extremely harsh conditions of high temperature (400 °C) and pressure (200 atm) to motivate the transformation of N_2 to NH_3 . Meanwhile, it also causes huge energy consumption and greenhouse emission to air in this process [2-7]. In principal producing NH_3 under mild conditions would address these issues if the efficiency is satisfactory [8]. Photocatalytic synthesis of NH_3 through fixing N_2 under ambient conditions is such a process that has attracted scientists' interests due to its safety, energy-saving,

economy and environmental friendship [9]. Although various semiconductors like SrTiO₃ [10], BaTiO₃ [11], CdS [2], BiOX [1, 12-15], g-C₃N₄ [16-19], and WO₃ [20, 21], have been developed as the photocatalysts for artificial synthesis of NH₃, TiO₂-based semiconductors are so far still considered to be the most stable, economical and robust photocatalysts [8]. Unfortunately, TiO₂-based photocatalyst suffered from low NH₃ synthesis activities because of fast electron-hole recombination and poor chemisorption of N₂ molecular. To solve these problems, oxygen vacancy construction [1, 8, 12, 22] and co-catalyst (eg. Ru [23], Pt [24], Au [25], Fe [26, 27], etc.) loading have been developed to promote N₂ chemisorption and activation, as well as improve charge carrier separations, thus leading to enhanced photocatalytic NH₃ synthesis activities.

In the recent years, Ti₃C₂ MXenes, a new kind of 2D layered material, without noble metal, has been widely used as a co-catalyst for the photocatalytic pollution elimination [28, 29], water splitting [30, 31], and CO₂ reduction [32, 33]. These reports in part proved that Ti₃C₂ MXenes are efficient and promising co-catalysts for enhancement of photocatalytic activity due to their excellent electrical conductivity and special 2D-layered structure with large surface area, which are all beneficial for the electron transfer and reactants chemisorption. More interesting, the reported DFT calculations pointed out Ti₃C₂ MXenes could be well combined with N₂, and thus can be considered as a good candidate to provide activation sites for N₂ activation [34].

Despite such attractive potential of Ti₃C₂ MXenes, there is no report to use Ti₃C₂ MXenes as a cocatalyst on NH₃ synthesis. Hence, this study targeted to immobilize Ti₃C₂ MXenes on the most robust photocatalyst P25 and then fully investigated its effect for photocatalytic NH₃ synthesis. Interestingly, the photocatalytic experiments show that 2D-layered Ti₃C₂ MXenes significantly improved the photocatalytic activity of P25 for NH₃ synthesis under ambient conditions. The mechanistic study and DFT calculations further reveal that 2D-layered Ti₃C₂ MXenes function by three means: i) a co-catalyst, the electro-chemical experiments and fluorescence spectra proved that 2D-layered Ti₃C₂ MXenes functioned as an electron acceptor in the separation and transformation of photon-generated carriers, ii) combination of Ti₃C₂ MXenes with P25 introduced the generation of oxygen vacancy on the surface of P25, which further facilitated N₂ chemisorption and activation, iii) DFT calculations demonstrated that the Ti₃C₂ MXenes are also effective chemisorption and activation materials of N₂ molecules. Therefore the

new photocatalyst for the first time demonstrated the function of 2D-layered Ti_3C_2 MXenes in NH_3 synthesis which could also be used in the related fields.

2. Experimental Section

2.1 Materials

P25 (composed of 80 % anatase, 20 % rutile, surface area: 50 m^2/g) was purchased from Degussa. Ti_3AlC_2 MAX phase powders (> 98 wt% purity) were purchased from Laizhou Kai Kai Ceramic Materials Co., Ltd. (Shandong, China). N_2 and Ar (both 99.999 %) were obtained from Xi'an tenglong chemical co. LTD. Ultrapure water was used in all experiments.

2.2 Synthesis of Ti_3C_2 MXenes

Ti_3C_2 MXenes were prepared by etching Ti_3AlC_2 MAX phase using HF (40%) solution[35]. In a typical synthesis, 2g Ti_3AlC_2 was mixed with 20 ml HF (40%) solution (with extra care) and stirred magnetically for 24 hours at room temperature. Then the reaction solution was centrifuged and continuously washed with ethanol and water until the supernatant was neutral. The sediment obtained was dried in 50 °C in vacuum over night.

2.3 Synthesis of Ti_3C_2 MXenes - P25

Certain amounts of Ti_3C_2 MXenes and 0.2 g P25 with a weight ratio of 2%, 4%, 6% and 8% were added to 30 mL ultra-pure water. After 1 hour's stirring and subsequent 1 hour's ultra-sonification, the solution was centrifuged and washed with ultra-pure water for several times. The obtained sediment was dried in vacuum at 50 °C, being followed by 3 hours' calcination in a tube furnace under N_2 atmosphere at 300 °C (heating rate of 5 °C/min). Then the obtained products were denoted based on the amounts of MXenes (2%, 4%, 6%, 8% Ti_3C_2 -P25).

2.4 Characterization:

Powder XRD patterns were performed by using Bruker D8 ADVANCE* with Cu-K α radiation ($\lambda = 1.5418 \text{ \AA}$). Raman spectra was collected on a Thermo DXR2 Raman spectrometer. Scanning electron microscopy (SEM) images were taken using a Hitachi SU8010 field-emission electron microscope. TEM and HRTEM images were taken on a Talos F200X field-emission

high-resolution transmission electron microscope operated at 200 kV. Photoluminescence spectra (PL) was measured at room temperature using a FLS-920 fluorescence spectrophotometer (Edinburgh Instruments Company, UK). UV-Vis diffuse reflectance spectra were recorded in the spectral region of 200-800 nm with a Shimadzu SolidSpec-3700 spectrophotometer, with BaSO₄ as the reflectance standard reference. The low temperature ESR spectra were recorded on a Bruker EXM EPR Spectrometer at 77 K. The XPS experiments were carried out by PHI 5000 VersaProbe II XPS system. All binding energies were referenced with respect to the C 1s peak (284.6 eV) of the surface adventitious carbon. The specific surface areas were determined using a surface analyzer (Tristar II3020) through nitrogen adsorption and desorption isotherms at 77 K by Brunauer-Emmett-Teller (BET) method.

2.5 Photocatalytic nitrogen fixation

The photocatalytic performance of MXenes - P25 samples with different ratios and reference samples (pristine P25 and MXenes) were evaluated using a 300 W Xe lamp (CEL, full spectrum) as the light source. 50 mg catalysts were dispersed ultrasonically in 70 mL ultrapure water and then the dispersion was added into quartz reactor with constant stirring, meanwhile high-purity N₂ was bubbled at a flow of 200 mL/min for 60 minutes in dark to obtain N₂ adsorption-desorption equilibrium. Subsequently, the Xe lamp was turned on and 1 mL detected sample solution was extracted by injection syringe at regular intervals. The ammonia concentrations were detected by ion chromatography (IC, SHINE CIC-D120) equipped with an Ionpac CS16 column (4 × 250 mm, Dionex), an suppressor (SHY-A/C), and a conductivity detector. The eluent was 30 mM CH₄O₃S solution; the flow rate was 0.5 mL/min; the suppress current was 50 mA. The retention time of NH₄⁺ is at about 11 min. The photocatalytic synthesis of NH₃ from N₂ molecular using CH₃OH as the proton source has the same procedure as above except 0.02 M methanol was added in the dispersion. Moreover, the content of N₂H₄ was tested colorimetrically using para-(dimethylamino) benzaldehyde [36]. The UV-Vis absorbance spectra of the colored samples formed in the colorimetric assays was acquired on a UV-3200 spectrophotometer (Shanghai MAPADA Instruments Co., Ltd). The amount of H₂ was determined by gas chromatography (GC-9790 II, FULI).

2.6 ¹⁵N₂ Isotope labeling experiments

An isotope labeling experiments were carried out to clarify the source of ammonia, by using both $^{14}\text{N}_2$ and $^{15}\text{N}_2$ as the feeding gas [37]. After the photocatalytic NH_3 synthesis by 6% Ti_3C_2 MXenes - P25 for 1 hour, the obtained $^{14}\text{NH}_3$ and $^{15}\text{NH}_3$ were distinguished by ^1H nuclear magnetic resonance (NMR, 600 MHz). The typical NMR signals of ^1H for $^{14}\text{NH}_4^+$ and $^{15}\text{NH}_4^+$ were detected using $^{14}\text{NH}_4\text{Cl}$ and $^{15}\text{NH}_4\text{Cl}$ as the standard sample. In this process, the prepared NH_3 solutions were concentrated before being added to deuterated DMSO.

2.7 Electrochemical tests

The electrochemical test was performed using a CHI-660 electrochemical station (Shanghai Chenhua, China) with a three-electrode cell. The glassy carbon electrode loaded catalyst was the working electrode, and saturated Ag/AgCl electrode and platinum foil were reference electrode and counter electrode, respectively. The electrochemical impedance spectroscopy (EIS) measurements were conducted over a frequency range 0.01-10⁵ Hz in 0.1M Na_2SO_4 electrolyte.

2.8 Photocurrent measurement

The photocurrent measurements were performed on a CHI 660 electrochemical station (Shanghai Chenhua, China) under irradiation of a 300-W Xe lamp (Solaredge 700, China). 5 mg as-prepared samples were ultrasonically dispersed in 485 μL ethanol and 500 μL water followed by 15 μL 5 wt % Nafion solution added. The suspension was then dip coated on 2 cm*1.5 cm FTO glass as the working electrode, and saturated Ag/AgCl electrode and platinum foil were the reference electrode and counter electrode, respectively. Photocurrent experiments were carried out under chopped light irradiation (light on/off cycles: 50 seconds) within 400 seconds in 0.1 M Na_2SO_4 electrolyte. The electrolyte was saturated with N_2 atmosphere during measurements.

2.9 DFT calculations

The density functional theory (DFT) calculations were performed using the spin-polarized projector augmented wave (PAW) pseudopotentials via the Vienna Ab initio Simulation Program (VASP) [38-41]. The crystal structure of TiO_2 and Ti_3C_2 were obtained from ICSD (TiO_2 : 154610; Ti_3C_2 : 95559). The exchange and correlation energies were treated using the generalized gradient approximation (GGA) via Perdew-Burke-Ernzerhof (PBE) prescription [42]. The constituted atomic valence states adopted were C $2s^22p^2$, N $2s^22p^3$, O $2s^22p^4$, and Ti $3p^63d^34s^1$. The plane

wave cut-off energy was 450 eV. A $7 \times 7 \times 3$ grid of Monkhorst-pack points were employed for geometry optimization of a 12-atom conventional cell of anatase TiO_2 [43], while a $3 \times 3 \times 1$ grid of Monkhorst-pack points were employed for geometry optimization of an 80-atom supercell of Ti_3C_2 (a hexagonal with an in-plane constant 12.33 Å) [44]. Geometry optimization were obtained by minimizing the total energy using a quasi-Newton algorithm to relax ions until it converged within 10^{-4} eV and the forces on each ion were less than $0.05 \text{ eV}/\text{Å}$. The Grimme DFT-D2 method was adopted to consider the van der Waals interactions (vdW), which is optimized for several DFT functional [44]. During the geometry optimization, volume and shape of the cell as well as atomic positions were relaxed.

For the anatase (101) surfaces as well as the surfaces which with an oxygen vacancy (S_{Ov}), A vacuum region of at least 15 Å was used so that the slabs in neighbouring cells in the vertical direction are separated by a sufficiently large distance. For the Ti_3C_2 surface, a vacuum of at least 15 Å is included in the supercell to avoid the spurious interaction. During the geometry optimization, the first three O-Ti-O-layers of the atoms were allowed to relax until reaching a 10^{-4} eV convergence in the total energy and the forces on each ion were less than $0.05 \text{ eV}/\text{Å}$, the three remaining O-Ti-O-layers were kept fixed (bulk like). To avoid the interaction among adsorbed molecules in neighboring cells, supercells with 10.3×15.2 Å units of surfaces are constructed.

We studied the most plausible N_2 adsorption configuration on the anatase (101) surface of TiO_2 and $\text{O}_v\text{-TiO}_2$. The geometry relaxations were performed in the same way as the perfect surface of TiO_2 (Figure S1), $\text{O}_v\text{-TiO}_2$ (Figure S2) and Ti_3C_2 (Figure S3).

The adsorption energy (E_{ads}) was calculated using the equation:

$$E_{\text{ads (TiO}_2\text{-N}_2)} = E_{(\text{N}_2@\text{slab})} - E_{\text{slab (TiO}_2)} - E_{(\text{N}_2)} \quad (1)$$

$$E_{\text{ads (Ti}_3\text{C}_2\text{-N}_2)} = E_{(\text{N}_2@\text{sur})} - E_{\text{sur (Ti}_3\text{C}_2)} - E_{(\text{N}_2)} \quad (2)$$

where $E_{(\text{N}_2@\text{slab})}$ is the total energy of TiO_2 (101) surface after N_2 adsorption, $E_{\text{slab (TiO}_2)}$ is the total energy of the TiO_2 (101) surface, $E_{\text{sur (Ti}_3\text{C}_2)}$ is the total energy of the Ti_3C_2 and $E_{(\text{N}_2)}$ the total energy of the isolated N_2 molecule.

3. Results and discussions

3.1 Characterization

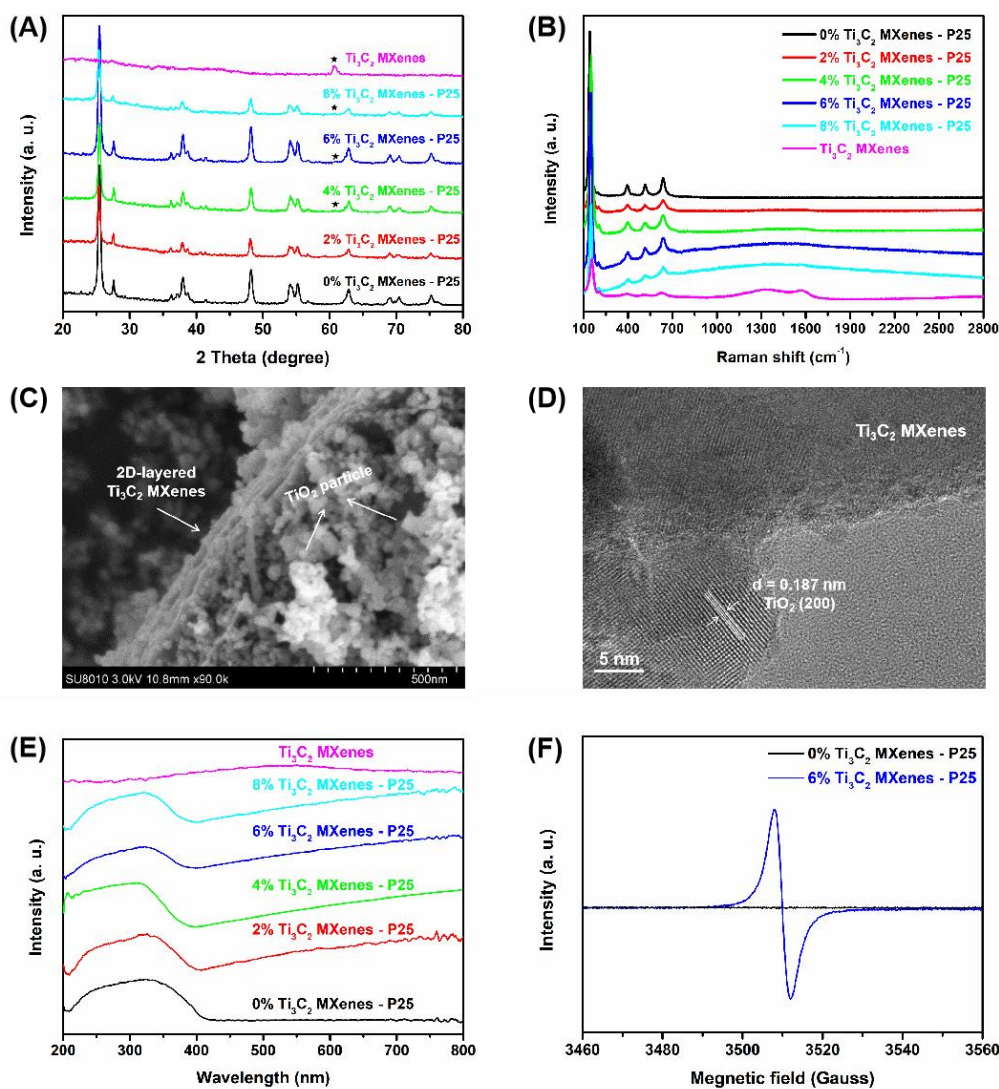


Figure 1 (A) XRD spectra of x% Ti_3C_2 MXenes - P25, asterisk indicates Ti_3C_2 ; an enlarged XRD were provided in Figure S4 and S5 to differentiate one from others, (B) Raman spectra of x% Ti_3C_2 MXenes -P25, (C) SEM image of 6% Ti_3C_2 MXenes - P25, (D) HRTEM image of 6% Ti_3C_2 MXenes -P25, (E) UV-vis DRS spectra of x% Ti_3C_2 MXenes - P25, (F) ESR spectra of 0% and 6% Ti_3C_2 MXenes - P25.

The XRD patterns of the prepared x% Ti_3C_2 MXenes - P25 samples are shown in Figure 1 (A). The diffraction peaks at 25.48° , 38.00° , 48.20° , 54.08° , 55.20° , 62.85° , 69.14° , 70.46° and

75.25° are corresponding to (101), (004), (200), (105), (211), (204), (116), (220), (215) crystal planes of anatase TiO₂ (JCPDS No. 21-1272) [45]. The peaks at 27.58°, 36.28°, 41.44° and 56.76° are consistent with the (110), (101), (111) and (220) facets of rutile TiO₂ (JCPDS No. 21-1276) [45]. In addition, the tiny peaks at about 61° for 4%, 6% and 8% Ti₃C₂ MXenes - P25 samples are ascribed to the (110) plane of Ti₃C₂ MXenes (JCPDS No. 32-1383) [46,47]. For more clear observation, enlarged image of P25, 8% Ti₃C₂ MXene-P25 and Ti₃C₂ MXene in range of 50 - 80° is also presented in Figure S4. These results ascertain for the co-existence of anatase TiO₂, rutile TiO₂ and Ti₃C₂ MXenes in the sample of Ti₃C₂ MXenes - P25. Further comparing the diffraction angles of P25 with the standard data in the range of 20 - 35°, somewhat right shifts are observed in these Ti₃C₂ MXenes - P25 samples (Figure S5). The right shifts point out the oxygen vacancies were introduced into the TiO₂ particles with the loading of Ti₃C₂ MXenes [48]. The oxygen vacancies may be formed with the migration of partial oxygen from P25, on the interface between P25 and Ti₃C₂ MXene, to Ti₃C₂ MXene during the calcination process in N₂ atmosphere. Figure 1 (B) shows the Raman spectra of all the x% Ti₃C₂ MXenes - P25 samples. For the sample of P25, the main peaks at about 145 cm⁻¹, 394 cm⁻¹, 512 cm⁻¹ and 638 cm⁻¹ are attributed to E_g, B_{1g}, A_{1g}, and E_g band mode of P25, respectively [32]. For Ti₃C₂ MXenes, the Raman peaks at 1363 cm⁻¹ and 1557 cm⁻¹ are assigned to D band and G band of carbon atoms [49]. The Raman spectra also indicate the composition of P25 and Ti₃C₂ MXenes in the composite samples. Meanwhile, broadening around 1500 cm⁻¹ for the composite samples is also related to the defects [49], consistent with the right shift of XRD patterns.

The morphology of composite samples are represented in Figure 1(C), 2D-layered structure of Ti₃C₂ MXenes can be clearly observed. Besides, we can also see that TiO₂ nanoparticles are anchored to 2D-layered Ti₃C₂ MXenes. The d-spacing of 0.187 nm in HRTEM image [Figure 1(D)] is corresponding to (200) plane of anatase TiO₂, which is somewhat smaller than the standard d-spacing (0.189 nm) of anatase TiO₂ (JCPDS No. 21-1272), indicating the introduction of oxygen vacancies [50]. The TEM also proves P25 particles embodied on 2D-layered Ti₃C₂ MXenes. The light absorption spectra of the prepared samples are compared in Figure 1 (E), the absorption edges at about 400 nm of all the samples are attributed to the intrinsic light absorption of TiO₂ [51]. The wide absorption of composite samples at the range of 400 - 650 nm is due to Ti₃C₂ MXenes

[32]. Furthermore, the increasing absorption of the composite samples from 400 nm to 800 nm is considered to stem from oxygen vacancies [52] and Ti_3C_2 MXene. The introduction of oxygen vacancies by Ti_3C_2 MXenes loading can also be proved by ESR spectra in Figure 1 (F). After loading Ti_3C_2 MXenes, a significant signal with a g value of 2.003 appears, which is the typical signal of oxygen vacancies [53].

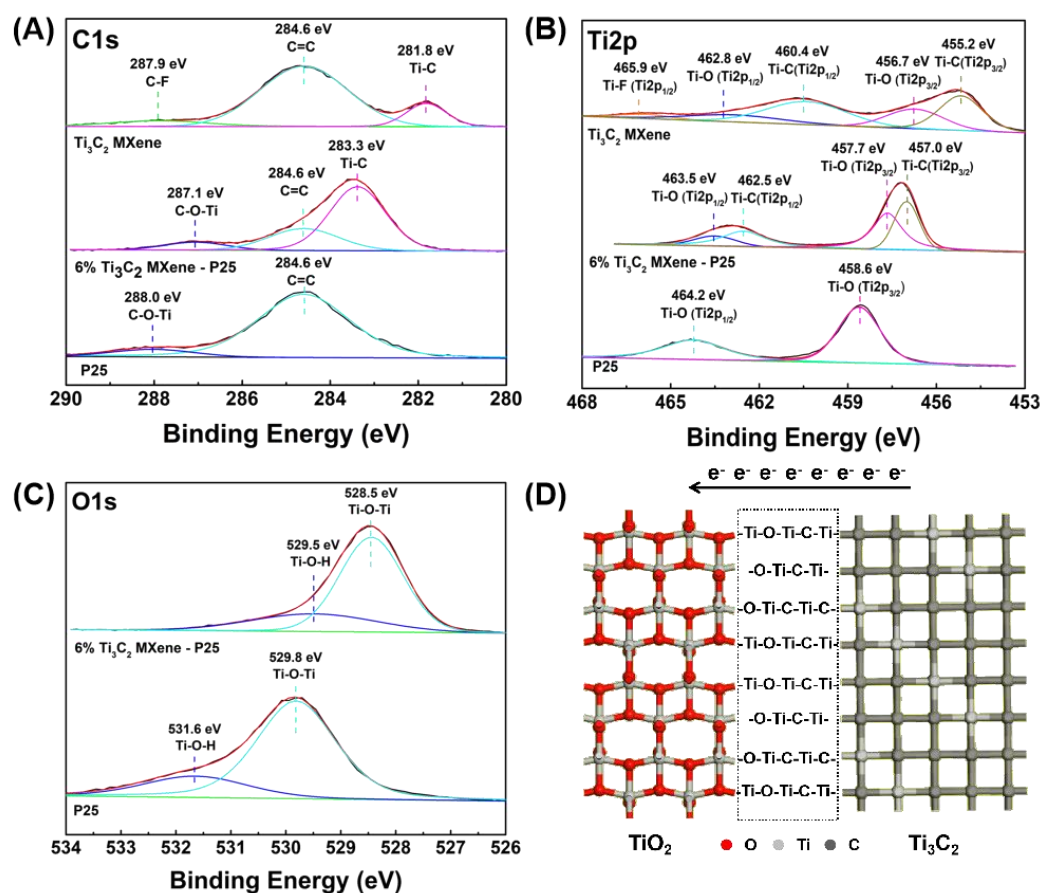


Figure 2 (A) C1s, (B) Ti2p, (C) O1s XPS spectra of P25, 6% Ti_3C_2 MXenes - P25, and Ti_3C_2 MXenes, (D) Diagram of the bond connection between TiO_2 and Ti_3C_2 MXenes.

The chemical states of C, O and Ti atoms in different samples were characterized by X-ray photoelectron spectroscopy (XPS). The high resolution XPS spectra of C1s in P25, 6% Ti_3C_2 MXenes - P25 and Ti_3C_2 MXenes are displayed in Figure 2 (A), while those of Ti2p and O1s in these samples are displayed in Figure 2 (B) and Figure 2 (C), respectively. For C1s XPS spectra, the peaks located at 284.6 eV in Figure 2 (A) are attributed to C1s of the amorphous C adsorbed on the surface of the prepared samples. The peaks at 288.0 eV and 287.1 eV in Figure 2 (A) are assigned to C-O-Ti bond of TiO_2 [48], while the peak at 287.9 eV is given to the C1s of C-F bond

in Ti_3C_2 MXenes [29]. The peaks of C1s at 283.3 eV and 281.8 eV [Figure 2 (A)] are ascribed to Ti-C bond of Ti_3C_2 MXenes. Then for Ti2p XPS spectra, two peaks at 464.2 eV and 458.6 eV in Figure 2 (B) are confirmed to Ti $2p_{1/2}$ and Ti $2p_{3/2}$ of typical Ti-O bond in P25 [49], while they are 463.5 eV (Ti $2p_{1/2}$) and 457.7 eV (Ti $2p_{3/2}$) in 6% Ti_3C_2 MXenes - P25. In addition, Ti $2p_{1/2}$ (462.5 eV) and Ti $2p_{3/2}$ (457.0 eV) of Ti-C bond are also observed in the XPS spectra of Ti2p for 6% Ti_3C_2 MXenes - P25 [49], different from those (Ti $2p_{1/2}$, 460.4 eV and Ti $2p_{3/2}$, 455.2 eV) existed in Ti_3C_2 MXenes [49]. The peaks at 462.8 eV and 456.7 eV are derived from Ti $2p_{1/2}$ and Ti $2p_{3/2}$ of Ti-O bond on the surface of Ti_3C_2 MXenes [49], and the peak at 465.9 eV are identified to Ti $2p_{3/2}$ of Ti-F bond [29]. Lastly for O1s XPS spectra, the peaks at 531.6 and 529.8 eV in Figure 2 (C) are corresponding to the O1s of Ti-O-H and Ti-O-Ti bond of P25, while they shift to 529.5 and 528.5 eV in the Ti_3C_2 MXenes - P25, respectively.

Significantly, the bonding energy of Ti-O in 6% Ti_3C_2 MXenes - P25 decreases compared with pure P25. On the other hand, the bonding energy of C-Ti in 6% Ti_3C_2 MXenes-P25 increases compared with that in Ti_3C_2 MXenes. These changes are originated from the O-Ti-C bond formation between TiO_2 and Ti_3C_2 MXenes, due to the larger electronegativity of O atom than that of C atom. Compared with O-Ti-O and C-Ti-C, the binding energies of all the atoms (O, Ti and C) in O-Ti-C have large shifts, as described in Figure 2. These XPS results in Figure 2 strongly indicate bonding between Ti_3C_2 MXenes and P25 occurred as described in Figure 2 (D).

3.2 Photocatalytic generation of NH_3

The photocatalytic synthesis of NH_3 from N_2 molecular by the as-prepared samples, with both H_2O and CH_3OH as proton sources, were carried out under full spectrum light irradiation. The experimental results, with H_2O as the proton source, are shown in Figure 3 (A). Upon full spectrum light irradiation for 1 hour, all samples with different loading amounts of Ti_3C_2 MXenes produce much more NH_3 than the parent samples pure P25 (2.11 $\mu\text{mol/g}$) and Ti_3C_2 MXenes (0.47 $\mu\text{mol/g}$). With the increase of Ti_3C_2 MXenes loading amount, the yield of NH_3 increases gradually (2%: 2.89 $\mu\text{mol/g}$ and 4%: 4.32 $\mu\text{mol/g}$). Subsequently, the highest is achieved when Ti_3C_2 MXenes loading amount reaches 6% (10.74 $\mu\text{mol/g}$), and then decreased when it is further increased to 8% (7.27 $\mu\text{mol/g}$). The highest NH_3 generation amount over 6% Ti_3C_2 MXenes - P25 is about 5 times higher than that over pure P25 and more than 20 times higher than Ti_3C_2 MXenes.

The BET surface area of 6% Ti_3C_2 MXenes was measured to be $34 \text{ m}^2/\text{g}$, lower than pure P25 ($50 \text{ m}^2/\text{g}$), but much higher than Ti_3C_2 MXenes ($0.6 \text{ m}^2/\text{g}$). Therefore such enhancement is attributed to the function of the cocatalyst other than surface area increase. This activity is also higher than that achieved by a Ru, a popular co-catalyst for photocatalytic NH_3 synthesis we reported before [54]. It is known that increasing loading amount of a co-catalyst can't always improve the photocatalytic activity of photocatalyst, as the excess co-catalyst will cover the surface of a photocatalyst and diminish its light absorption [55]. Meanwhile, the control experiments were also carried. As we can see in Figure S6, NH_3 is either hardly produced or negligible in the absence of full spectrum light, N_2 or the photocatalyst. These results in part suggest that N atoms in the produced NH_3 come from N_2 molecules we added in the reaction system. Moreover, the cycling experiments were also conducted to prove the stability and repeatability of the photocatalyst, which are of great significance for practical applications. Figure 3 (B) shows that little decrease of NH_3 generation yields occurred after three cycles. This small change of the activity between cycles is believed to be due to the loss of the mass of the photocatalyst when recycling the photocatalyst. Regarding the selectivity of NRR, we tested the production of N_2H_4 and H_2 , the results show that there is no N_2H_4 (Figure S7) and H_2 produced during photocatalytic nitrogen fixation, indicating good selectivity of the catalyst for N_2 reduction reaction over H_2 . This excellent selectivity is due to two reasons. One is much stronger adsorption of N_2 ($\Delta G_{\text{N}_2} < -1.35 \text{ eV}$) [34] than that of H atom ($\Delta G_{\text{H}^*} > -0.927 \text{ eV}$) [30] on the surface of Ti_3C_2 MXene. The other is because the photoelectrons on Ti_3C_2 MXe have a weak reduction potential, very close to H^+/H_2 potential, while much more negative than N_2/NH_3 [56] as indicated in Scheme 1, so they could reduce N_2 to NH_3 but hard to reduce proton to H_2 gas. These results suggest that Ti_3C_2 MXenes - P25 possesses a reasonable stability and selectivity for photocatalytic NH_3 synthesis from N_2 under present conditions.

Then the photocatalytic synthesis of NH_3 over the as-prepared Ti_3C_2 MXenes - P25 using CH_3OH as the proton source and a hole scavenger were also performed, under full spectrum light irradiation. Similar trends are observed in Figure 3 (C) - (D) while all samples behave much better. Obviously, 6% Ti_3C_2 MXenes - P25 produces 4 times higher activity ($43.44 \mu\text{mol/g}$) than that using water as the proton source. This enhancement is due to higher efficiency of methanol as a

hole scavenger than water (10.74 $\mu\text{mol/g}$). Again the photocatalytic generation of NH_3 by P25 is efficiently improved by Ti_3C_2 MXenes loading. Enhanced by Ti_3C_2 loading, our Ti_3C_2 MXenes - P25 catalyst exhibits excellent photocatalytic performance for N_2 fixation (Table S1).

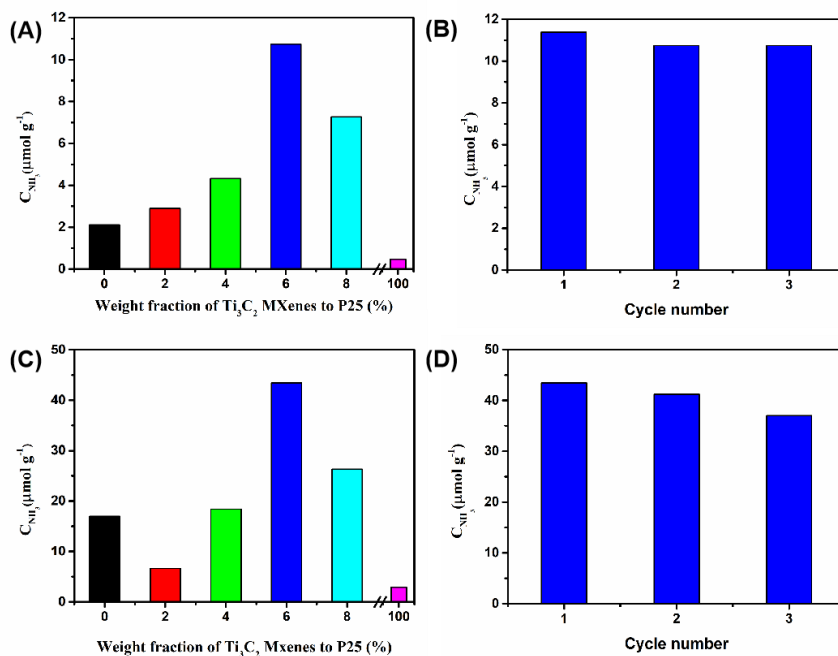


Figure 3 (A) Yields of NH_3 on different samples of x% Ti_3C_2 MXenes - P25 after 1 hour irradiation, with H_2O as the proton sources, (B) Cycling experiments of NH_3 synthesis over 6% Ti_3C_2 MXenes -P25 for 1 hour irradiation, with H_2O as the proton source, (C) Yields of NH_3 by different samples of x% Ti_3C_2 MXenes - P25 after 1 hour irradiation, with CH_3OH as the proton source, (D) Cycling experiments of NH_3 synthesis over 6% Ti_3C_2 MXenes -P25 for 1 hour irradiation, with CH_3OH as the proton source.

3.3 Mechanism

Furthermore, we compared the NH_3 yields by P25 and 6% Ti_3C_2 MXenes - P25 with H_2O or CH_3OH as the hole scavenger, respectively. One can see in Figure 4 (A), the NH_3 yield in 1 hour over 6% Ti_3C_2 MXenes - P25 is 5 times higher than that over P25 in the presence of H_2O , while it is only 1.4 times higher when CH_3OH was as the proton source and hole scavenger. With H_2O as the proton source and the hole scavenger, Ti_3C_2 MXenes is proposed to help charge separation and promote N_2 adsorption as discussed later. With CH_3OH as the proton source, Ti_3C_2 MXenes acts only to promote N_2 adsorption as CH_3OH is a well known hole scavenger to facilitate efficient

electron-hole separation. When photogenerated electrons and holes are produced under illumination, the holes will be fast trapped by methanol and consumed, resulting in a better charge separation and then a more efficient photocatalytic performance of NH₃ synthesis. These results indicate that Ti₃C₂ MXenes likely not only enhance the separation of photogenerated electron-hole pairs generated in P25, but also promote the N₂ chemisorption and activation during the photocatalytic synthesis of NH₃ under full spectrum light irradiation.

To give a more powerful evidence of the N source, isotope labeling experiments were further performed with ¹⁴N₂ and ¹⁵N₂ as the feeding gas, respectively. The products were identified by NMR spectra of ¹H. According to earlier literature [37], H atoms would be divided to several peaks by N atom, and the number of peaks is decided by the statement of $2nI + 1$. Here, n is the number of N atom, and I represents the spin quantum number of isotope N, herein $I = 1$ for ¹⁴N and $I = 1/2$ for ¹⁵N. The reference sample shown in Figure S9 presents that the peak of H in NMR spectra is divided to 3 peaks by ¹⁴N, while it is 2 peaks by ¹⁵N. In addition, the coupling constant of the triple peaks is 52.3 Hz for ¹⁴NH₄⁺, while that of double peaks is 73.2 Hz for ¹⁵NH₄⁺. Significantly, both similar number of peaks and the coupling constants results were obtained in Figure 4 (B) when we used ¹⁴N₂ and ¹⁵N₂ as the feeding gas, strongly supporting that N₂ molecular we fed in the solution is indeed the N source of NH₃ synthesis by photocatalysis in this work.

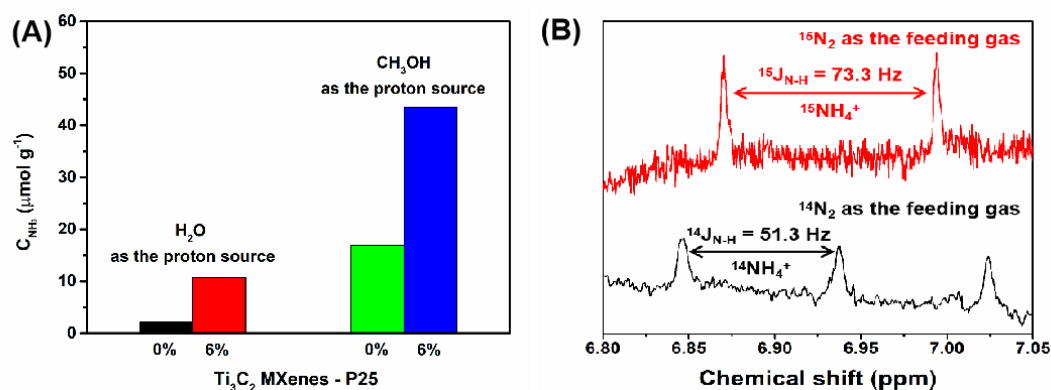


Figure 4 (A) Yields of NH₃ in 1 hour on 0% and 6% Ti₃C₂ MXenes - P25 with H₂O and CH₃OH as the proton source; (B) ¹H NMR spectra of ¹⁵NH₄⁺ and ¹⁴NH₄⁺ ions produced by 6% Ti₃C₂ MXenes - P25 using ¹⁵N₂ and ¹⁴N₂ as the feeding gas.

In order to investigate the generation and migration of photoinduced charge carriers, photocurrent densities and electrochemical impedance of all the samples were measured. As

displayed in Figure 5 (A), all Ti_3C_2 MXenes - P25 samples have higher photocurrent densities than pure P25. Significantly, the photocurrent density of 6% Ti_3C_2 MXenes - P25 is nearly 6 times larger than P25, almost consistent with the 5 times enhancement in NH_3 synthesis.. For electrochemical impedance spectra, smaller diameter of the semi-circle in a Nyquist plot represents smaller charge-transfer resistance for a photocatalyst. Thus, the data in Figure 5 (B) shows that the semi-circle diameter of 6% Ti_3C_2 MXenes - P25 sample is the smallest among all the samples, indicating the smallest resistance and most efficient charge carrier migration.

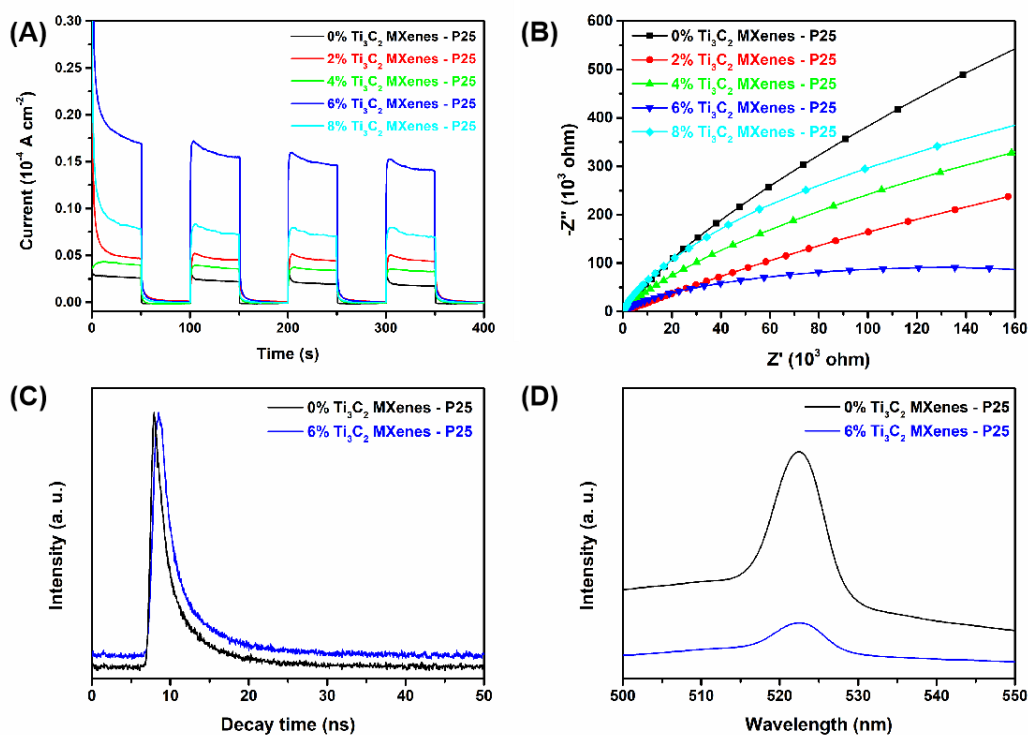


Figure 5 (A) Photocurrent responses of x% Ti_3C_2 MXenes - P25; (B) Electrochemical impedance spectra Nyquist plots of x% Ti_3C_2 MXenes - P25; (C) Transient state fluorescence spectra of 0% and 6% Ti_3C_2 MXenes - P25; (D) Steady state fluorescence spectra of 0% and 6% Ti_3C_2 MXenes - P25.

To further rationalize the charge transfer, the promoting effect of Ti_3C_2 MXenes on P25 was also investigated by the transient and steady state fluorescence spectra. The transient state fluorescence spectra of 0% and 6% Ti_3C_2 MXenes - P25 were measured and displayed in Figure 5 (C). In Table S2, τ_1 and τ_2 are the decay time, while B_1 and B_2 are the corresponding coefficient. τ_1 , τ_2 , B_1 and B_2 were obtained by fitting the decay time curve by a double - exponential mode. Of

which, fast attenuation component τ_1 represents the radiative emission via direct inter-band exciton recombination, while low attenuation component τ_2 involves the radiative emission of indirect recombination of trapped electrons with valence band holes [1]. In detailed, higher proportion of long-living component ($B_2\tau_2$: 49.57% for P25; 43.62% for 6% Ti_3C_2 MXenes - P25) suggests that indirect recombination of trapped electrons with the valence band holes dominates the exciton recombination process. Based on these data, we calculated the average lifetimes (τ) of 0% and 6% Ti_3C_2 MXenes - P25 by the equation of $\tau = (B_1\tau_1^2 + B_2\tau_2^2)/(B_1\tau_1 + B_2\tau_2)$, respectively. The photocarriers' lifetime of 6% Ti_3C_2 MXenes - P25 (4.14 ns) is also significantly longer than that of pure P25 (3.72 ns). This result suggests that the photocarriers in 6% Ti_3C_2 MXenes - P25 have longer time than those in pure P25, resulting in a lower recombination rate. Then, broad emission peaks centered at about 523 nm were observed over both 0% and 6% Ti_3C_2 MXenes - P25 samples in Figure 5 (D). These peaks are considered to be arisen from the radiative emission of indirect recombination of the trapped electrons with the valence band holes, according to the conclusion obtained from the above transient state fluorescence spectra. Compared to pure P25, 6% Ti_3C_2 MXenes - P25 shows 5 times lower fluorescence intensity, indicating a higher separation rate of electron-hole pairs.

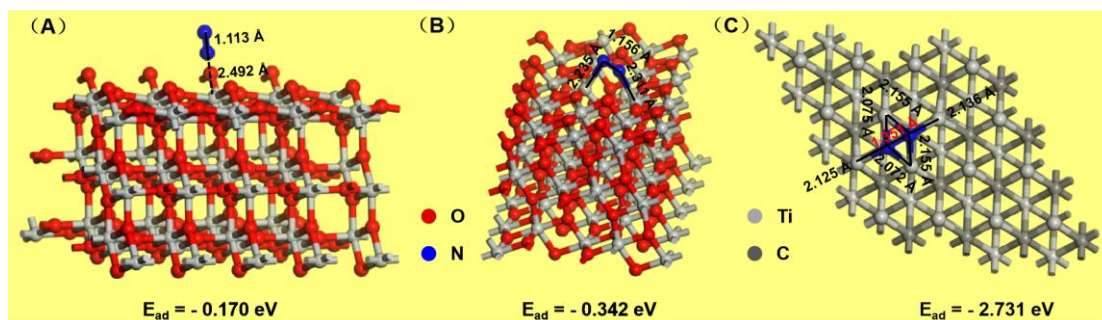
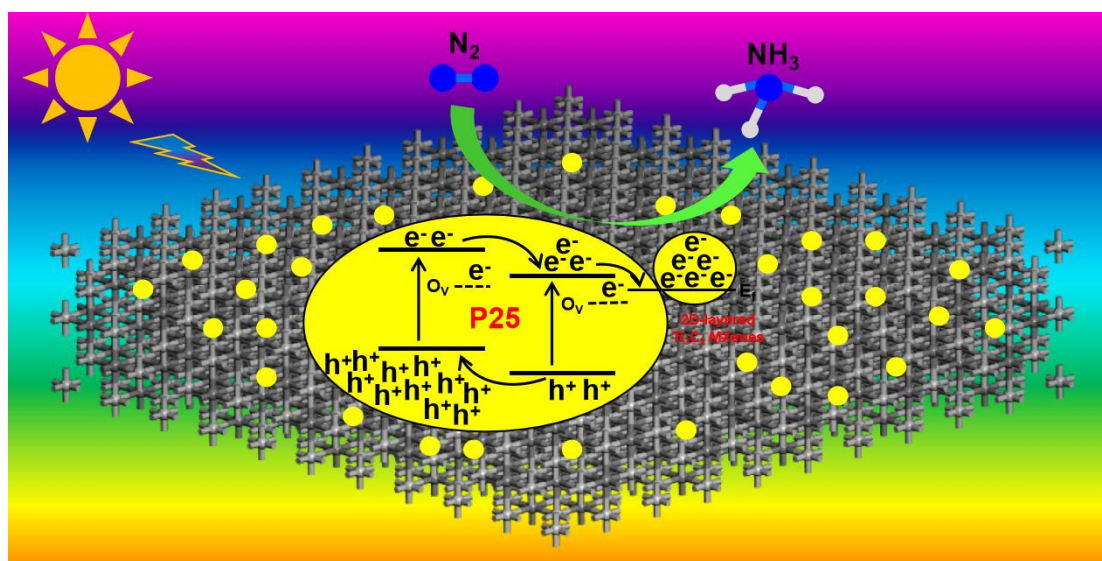


Figure 6 Schematics of slab model after relaxation for N_2 @5-fold-Ti (A) and N_2 @4-fold-Ti (B).
(C) Schematics of slab model after relaxation for N_2 @ Ti_3C_2 MXenes.

It is worth to note that the chemisorption of N_2 molecular on the surface of photocatalyst is crucial for the symmetric molecules' activation. Accordingly, DFT calculation was used to evaluate the adsorption energy and the length of $\text{N}\equiv\text{N}$ on the surface of different samples, which are critical considerations during the synthesis process of NH_3 . Notably, the adsorption energies of N_2 on the surface of TiO_2 , V_O - TiO_2 and Ti_3C_2 MXenes, corresponding to the optimized adsorption

structures, are shown in Figure 6. The calculated adsorption energies are ranked as Ti_3C_2 MXenes (2.731 eV) > V_O - TiO_2 (0.342 eV) > TiO_2 (0.170 eV), meaning that much stronger chemisorption effect occurs between N_2 and Ti_3C_2 MXenes, compared to V_O - TiO_2 and TiO_2 . Furthermore, higher adsorption energies should weaken the $\text{N}\equiv\text{N}$ triple bond, resulting in elongated $\text{N}\equiv\text{N}$ bond and shorter distances between Ti and N atoms. As proved in Figure 6, the length sequence of $\text{N}\equiv\text{N}$ triple bond is consistent with the adsorption energy, which is Ti_3C_2 MXenes (1.351 Å) > V_O - TiO_2 (1.156 Å) > TiO_2 (1.113 Å). Correspondingly, the distances sequence of Ti-N is reversed: N_2 - Ti_3C_2 MXenes (2.125 Å, 2.136 Å, 2.075 Å, 2.072 Å, 2.155 Å, 2.155 Å) < N_2 - V_O - TiO_2 (2.235 Å, 2.311 Å) < N_2 - TiO_2 (2.492 Å). These results mean that the activation of N_2 molecular on the surface of Ti_3C_2 MXenes is thermodynamically much readily than those on the surface of V_O - TiO_2 and pure TiO_2 , strongly supporting Ti_3C_2 MXenes as an efficient co-catalysts for the photocatalytic NH_3 synthesis from N_2 molecules. Meanwhile, oxygen vacancies introduction is also a useful strategy for the photocatalytic NH_3 synthesis although it is not as useful as the cocatalyst.



Scheme 1 Schematic illustration for the promotion effect of 2D-layered Ti_3C_2 MXenes on P25 for photocatalytic NH_3 synthesis from N_2 molecular.

The photocatalytic activity is closely related to the surface interfacial properties because the photocatalytic reaction mainly occurs on the surface of photocatalysts. Based on the discussions above, oxygen vacancies were successfully introduced in P25 by Ti_3C_2 MXenes loading process, and defect states induced by oxygen vacancies would in part retard the electron-hole

recombinations reported [52]. To further verify this hypothesis, ESR spectra of 6% Ti_3C_2 MXenes - P25 were further performed in Ar and N_2 atmosphere, respectively. As observed in Figure S10, the characteristic signal of oxygen vacancies in N_2 is obviously weaker than that in Ar, indicating a reaction of N_2 molecules with the photocatalyst. Furthermore the Fermi level of Ti_3C_2 MXenes (-0.04 V vs. NHE) is obviously less negative than the conduction band of TiO_2 (-0.25 V vs. NHE) and we believe that MXene and MXene/ TiO_2 heterocatalyst have similar work function, determined by the Fermi level of MXene. This suggests that the photogenerated electrons on the conduction band of TiO_2 are feasible to migrate to Ti_3C_2 MXenes (Scheme 1). Sequentially, Ti_3C_2 MXenes can effectively hold the free electrons from P25 due to its high electric capacity, excellent electrical conductivity, and 2D-layered structure. As a result, the separation of electron-hole pairs is efficiently promoted, resulting in a long lived photoelectrons for the subsequent chemical reaction. Next, Ti_3C_2 MXenes are important for chemisorption and activation of N_2 molecules, according to the results of DFT calculations. The redox potential for nitrogen reduction reaction to produce ammonium is 0.55V vs NHE according to the earlier review [56]. Theoretically, the work function of one photocatalyst should be more negative than standard redox potential of NRR (0.55V vs NHE) as an overpotential is also required. Our current results indicate that a work function of nearly 0 V vs. NHE is enough for the NRR reaction. Overall, Ti_3C_2 MXenes are efficient co-catalysts for the photocatalytic synthesis of NH_3 .

4. Summary

In summary, Ti_3C_2 MXene was successfully used as a new co-catalyst in the photocatalytic synthesis of NH_3 from N_2 under ambient conditions. The production of NH_3 by P25 was efficiently promoted by Ti_3C_2 MXenes loading under light irradiation. The highest photocatalytic activity was achieved on 6% Ti_3C_2 MXenes-P25 sample, resulting into 5 times higher than pure P25 although the former has a much smaller surface area. This is consistent with 5 times enhancement in photocurrent densities experiments. The important roles of Ti_3C_2 MXenes have been thoroughly investigated. Ti_3C_2 MXenes loading process introduced oxygen vacancies doped in P25, which not only decrease the recombination of excited electron-hole pairs, but also promote the adsorption N_2 molecules on the photocatalyst. More importantly, Ti_3C_2 MXenes play an important role for the separation of photogenerated electron-hole pairs by storing the electrons

from the excited P25 substrate and for chemisorption and activation of N₂ molecules. Finally Ti₃C₂ MXenes can accelerate the reaction between the adsorbed N₂ and stored photoelectrons. In total this study provides an efficient and promising co-catalyst for photocatalytic NH₃ synthesis process from N₂ in air either using water or methanol as the proton source and the hole scavenger.

Acknowledgement

Y. L., J. Q., G. X., Y. W., S. Z., L. L., W. Z. and H.-Y. J. are grateful for the financial supports of National Natural Science Foundation of China (No. 21703170), Yong Academic Talents Program of Northwest University and Top-rated Discipline construction scheme of Shaanxi higher education. J. W. T. and Q. H. are thankful for financial support from UK EPSRC (EP/N009533/1), Royal Society-Newton Advanced Fellowship grant (NA170422) and the Leverhulme Trust (RPG-2017-122).

References

- [1] H. Li, J. Shang, Z. Ai, L. Zhang, *J. Am. Chem. Soc.* 132 (2015) 6393-6399.
- [2] K. A. Brown, D. F. Hrris, M. B. Wilker, A. Rasmussen, N. Khadka, H. Hamby, S. Keable, G. Dukovic, J. W. Peters, L. C. Seefeldt, P. W. King, *Science* 352 (2016) 448-450.
- [3] T. Rayment, R. Schlogl, J. M. Thomas, G. Ertl, *Nature* 315 (1985) 311-313.
- [4] D. E. Canfield, A. N. Clazer, P. G. Falkowski, *Science* 330 (2010) 192-196.
- [5] C. J. M. Van der Ham, M. T. M. Koper, D. G. H. Hetterscheid, *Chem. Soc. Rev.* 43 (2014) 5183-5191.
- [6] C. Guo, J. Ran, A. Vasileff, S.-Z. Qiao, *Energy Environ. Sci.* 11 (2018) 45-56.
- [7] D. Zhu, L. Zhang, R. E. Ruther, R. J. Hamers, *Nat. Mater.* 12 (2013) 836-841.
- [8] Y. Zhao, Y. Zhao, R. Shi, B. Wang, G. I. M. Waterhouse, L.-Z. Wu, C.-H. Tung, T. Zhang, *Adv. Mater.* 31 (2019) 1806482.
- [9] T. Oshikiri, K. Ueno, H. Misawa, *Angew. Chem.* 128 (2016) 4010-4014.
- [10] T. Oshikiri, K. Ueno, H. Misawa, *Angew. Chem. Int. Ed.* 53 (2014) 9802-9805.

- [11] Q.-S. Li, K. Domen, S. Naito, T. Onishi, K. Tamaru, *Chem. Lett.* 12 (1983) 321-324.
- [12] S. Wang, X. Hai, X. Ding, K. Chang, Y. Xiang, X. Meng, Z. Yang, H. Chen, J. Ye, *Adv. Mater.* 29 (2017) 1701774.
- [13] H. Li, J. Shang, J. Shi, K. Zhao, L. Zhang, *Nanoscale* 8 (2016) 1986-1993.
- [14] Y. Bai, L. Ye, T. Chen, L. Wang, X. Shi, X. Zhang, D. Chen, *ACS Appl. Mater. Interfaces* 8 (2016) 27661-27668.
- [15] Y. Wang, W. Wei, M. Li, S. Hu, J. Zhang, R. Feng, *RSC Adv.* 7 (2017) 18099-18107.
- [16] G. Dong, W. Ho, C. Wang, *J. Mater. Chem. A* 3 (2015) 23435-23441.
- [17] S. Hu, Y. Li, F. Li, Z. Fan, H. Ma, W. Li, X. Kang, *ACS Sustainable Chem. Eng.* 4 (2016) 2269-2278.
- [18] Q. Zhang, S. Hu, Z. Fan, D. Liu, Y. Zhao, H. Ma, F. Li, *Dalton Trans.* 45 (2016) 3497-3505.
- [19] S. Hu, W. Zhang, J. Bai, G. Lu, L. Zhang, G. Wu, *RSC Adv.* 6 (2016) 25695-25702.
- [20] H. Liang, H. Zou, S. Hu, *New J. Chem.* 41 (2017) 8920-8926.
- [21] Y. Liu, M. Cheng, Z. He, B. Gu, C. Xiao, T. Zhou, Z. Guo, J. Liu, H. He, B. Ye, B. Pan, Y. Xie, *Angew. Chem. Int. Ed.* 58 (2019) 731-735.
- [22] H. Hirakawa, M. Hashimoto, Y. Shiraishi, T. Hirai, *J. Am. Chem. Soc.* 139 (2017) 10929-10936.
- [23] K. T. Ranjit, T. K. Varadarajan, B. Viswanathan, *J. Photochem. Photobiol. A* 96 (1996) 181-185.
- [24] K. Hoshino, *Chem.-Eur. J.* 7 (2001) 2727-2731.
- [25] C. M. Janet, S. Navaladian, B. Viswanathan, T. K. Varadarajan, R. P. Viswanath, *J. Phys. Chem. C* 114 (2010) 2622-2632.
- [26] T. Oshikiri, Ueno, Kosei, H. Misawa, *Angew. Chem. Int. Ed.* 53 (2014) 9802-9805.
- [27] Y. Lu, Y. Yang, T. Zhang, Z. Ge, H. Chang, P. Xiao, Y. Xie, L. Hua, Q. Li, H. Li, B. Ma, N.

- Guan, Y. Ma, Y. Chen, ACS Nano 10 (2016) 10507-10515.
- [28] H. Zhang, M. Li, J. Cao, Q. Tang, P. Kang, C. Zhu, M. Ma, Ceram. Int. 44 (2018) 19958-19962.
- [29] T. Cai, L. Wang, Y. Liu, S. Zhang, W. Dong, H. Chen, X. Yi, J. Yuan, X. Xia, C. Liu, S. Luo, Appl. Catal. B: Environ. 239 (2018) 545-554.
- [30] J. Ran, G. Gao, F.-T. Li, T.-Y. Ma, A. Du, S.-Z. Qiao, Nat. Commun. 8 (2017) 13907.
- [31] Y. Li, X. Deng, J. Tian, Z. Liang, H. Cui, Appl. Mater. Today 13 (2018) 217-227.
- [32] J. Low, L. Zhang, T. Tong, B. Shen, J. Yu, J. Catal. 361 (2018) 255-266.
- [33] M. Ye, X. Wang, E. Liu, J. Ye, D. Wang, ChemSusChem. 11 (2018) 1606-1611.
- [34] L. M. Azofra, N. Li, D. R. MacFarlane, C. Sun, Energy Environ. Sci. 9 (2016) 2545-2549.
- [35] Y. Fang, Z. Liu, J. Han, Z. Jin, Y. Han, F. Wang, Y. Niu, Y. Wu, Y. Xu, Adv. Energy Mater. 9 (2019) 1803406.
- [36] S. Zhang, Y. Zhao, R. Shi, C. Zhou, G. I. N. Waterhouse, L.-Z. Wu, C.-H. Tung, T. Zhang, Adv. Energy Mater. 10 (2020) 1901973.
- [37] L. Zhang, L.-X.; Ding, G.-F. Chen, X. Yang, H. Wang, Angew. Chem. Int. Ed. 58 (2019) 2612-2616.
- [38] P. Hohenberg, W. Kohn, Phys. Rev., 136 (1964) B864
- [39] P. E. Blöchl, Phys. Rev. B 50 (1994) 17953.
- [40] G. Kresse, D. Joubert, Phys. Rev. B 59 (1999) 1758.
- [41] G. Kresse, J. Furthmüller, Phys. Rev. B 54 (1996) 11169.
- [42] J. P. Perdew, K. Burke, M. Ernzerhof, Phys. Rev. Lett. 77 (1996) 3865.
- [43] H. J. Monkhorst, J. D. Pack, Phys. Rev. B 13 (1976) 5188.
- [44] S. Grimme, J. Comput. Chem. 27 (2006) 1787.

- [45] Slamet, Setiadi, D. Tristantini, E. Kusriani, D. Philo, *Int. J. Ind. Chem.* 9 (2018) 127-139.
- [46] K. Wang, Y. Zhou, W. Xu, D. Huang, Z. Wang, M. Hong, *Ceram. Int.* 42 (2016) 8419-8424.
- [47] M. Ghidui, M. R. Lukatskaya, M.-Q. Zhao, Y. Gogotsi, M. W. Barsoum, *Nature* 516 (2014) 78-81.
- [48] S. Chen, Y. Xiao, Y. Wang, Z. Hu, H. Zhao, W. Xie, *Nanomater.* 8 (2018) 245.
- [49] W. Yuan, L. Cheng, Y. Zhang, H. Wu, S. Lv, L. Chai, X. Guo, L. Zheng, *Adv. Mater. Interfaces* 4 (2017) 1700577.
- [50] S. Hu, P. Qiao, L. Zhang, B. Jiang, Y. Gao, F. Hou, B. Wu, Q. Li, Y. Jiang, C. Tian, W. Zhou, G. Tian, H. Fu, *Appl. Catal. B: Environ.* 239 (2018) 317-323.
- [51] K. Cheng, W. Sun, H.-Y. Jiang, J. Liu, J. Lin, *J. Phys. Chem. C* 117 (2013) 14600-14607.
- [52] H. Song, C. Li, Z. Lou, Z. Ye, L. Zhu, *ACS Sustainable Chem. Eng.* 5 (2017) 8982-8987.
- [53] J. Wan, W. Chen, C. Jia, L. Zheng, J. Dong, X. Zheng, Y. Wang, W. Yan, C. Chen, Q. Peng, D. Wang, Y. Li, *Adv. Mater.* 30 (2018) 1705369.
- [54] Y. Liao, J. Lin, B. Cui, G. Xie, S. Hu, *J. Photochem. Photobio. A: Chem.* 387 (2010) 112100.
- [55] H.-Y. Jiang, G. Liu, M. Li, J. Liu, W. Sun, J. Ye, J. Lin, *Appl. Catal. B: Environ.* 163 (2015) 267-276.
- [56] X. Chen, N. Li, Z. Kong, W.-J. Ong, X. Zhao, *Mater. Horiz.* 5 (2018) 9-27.